Properties of high-T_c Josephson junctions with $Y_{0.7}Ca_{0.3}Ba_2Cu_3O_{7-\delta}$ barrier layers
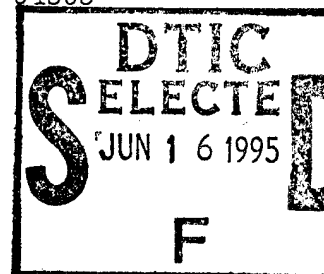
L. Antognazza, B. H. Moeckly, T. H. Geballe*, and K. Char

Conductus Inc., Sunnyvale, California   94086
* *also at Dept. of Applied Physics, Stanford University, Stanford, California 94305*

Abstract

We report the use of $Y_{0.7}Ca_{0.3}Ba_2Cu_3O_{7-\delta}$ as an epitaxial barrier between $YBa_2Cu_3O_{7-\delta}$ (YBCO) electrodes in high-T_c SNS edge junctions. Ca-doped YBCO is an overdoped version of YBCO, and it has an excellent lattice and thermal expansion match with YBCO. We show that these junctions exhibit clean interfaces with resistances smaller than 10^{-10} Ω cm^2. We present the temperature dependence of the critical current density J_c and the junction resistance R_n for junctions with 200 Å, 400 Å, and 600 Å thick barriers of $Y_{0.7}Ca_{0.3}Ba_2Cu_3O_{7-\delta}$. As the temperature decreases, the resistance of the junction decreases faster than the resistance calculated from the resistivity of a $Y_{0.7}Ca_{0.3}Ba_2Cu_3O_{7-\delta}$ film. We analyze our data by considering various possibilities for the microstructure in the barrier region. We discuss the ideal conventional proximity effect, diffusion between the barriers and the electrodes, and doping fluctuations inside the barrier. We find that combinations of these ideas explain the observed behavior with reasonable parameters.

Pacs: 74.50.+r , 74.76.-w , 74.80.Fp

19950613 003

March 20, 1995

I. Introduction

High temperature superconductor-normal-superconductor (SNS) Josephson junctions have attracted considerable attention because of their possible electronic applications, such as ultra fast digital logic circuits and shift registers or their use in SQUIDs. Josephson junctions also provide an elegant method to test phenomena like the proximity effect [1] or to investigate such issues as the wave function symmetry of YBCO [2, 3, 4]. In order to use these junctions as a model system, especially for investigation of a possible high-T_c proximity effect, the junction interfaces must be clean, i.e. the interface resistances at the S-N boundaries should be very small. The important problem of interface resistance in high-T_c junctions has indeed been recognized for some time. For instance, junctions made with Au or Ag [5], $CaRuO_3$, [6] and $SrRuO_3$ [7] as a barrier are known to have interface resistances of the order of 10^{-8}–10^{-7} $\Omega \cdot cm^2$, similar to the values observed in grain-boundary weak links. These high values influence the junction parameters, such as the magnitude and reproducibility of the critical current I_c, which limit the applicability of such junctions in electronic circuits. The origin of the high resistance in both SNS and grain-boundary junctions is believed to be oxygen deficient or oxygen disordered YBCO adjacent to the interface [8,9]. We have shown recently that the mismatch of thermal expansion coefficients at the S-N interface may be a contributing factor to the excess interface resistance [8]. An evident way to avoid this problem is to use a barrier material which is both epitaxial and has a matching coefficient of expansion. This goal can be achieved by using barriers which have the same layered structure as YBCO but with a lower T_c. The doped YBCO system is thus an excellent candidate.

In recent articles [8, 10] we have reported that junctions with barriers of $YBa_2(Cu_{1-x}Co_x)_3O_{7-\delta}$ and $Y_{0.7}Ca_{0.3}Ba_2Cu_3O_{7-\delta}$ have interface resistances as low as

March 20, 1995

A-1

10^{-10} $\Omega \cdot cm^2$, i.e. two orders of magnitude lower than grain boundaries or junctions made with Au, Ag, and $CaRuO_3$ [5, 6]. Those low interface resistances have been reproduced in the edge junction geometry with Co-doped YBCO by Koren *et al.* [11] and in the Ca-doped YBCO system by Jia *et al.* [12]. Our previous study showed that for Co-doped YBCO junctions, the temperature dependencies of R_n and I_c are different from junctions which have higher interface resistances [5]. Furthermore, we have demonstrated that the $I_c(T)$ curves can be well described by the framework of de Gennes' proximity effect theory [13].

It is important to recognize, however, that these results have only been obtained with *superconductor* barrier materials operating above their T_c. Furthermore, the Co-doped YBCO junctions utilized an *underdoped* version of YBCO as the barrier, and it will be useful for the understanding of SNS junctions to know how the properties of the junctions can be affected by the carrier density of the barrier. In order to address this latter point, we present the properties of SNS junctions with barriers of Ca-doped YBCO, which is an *overdoped* version of YBCO. Although we will show that some of the properties of these Ca-doped YBCO junctions can be understood within the de Gennes theory, they can also be explained by models invoking diffusion and percolation. This follows from the fact that the barrier itself is a superconductor with a reduced T_c, together with the recognition of a possible inhomogeneous distribution of oxygen and/or other defects on a length scale bigger than the superconductor coherence length ξ, a point for which we present some evidence.

II. Experimental Procedure

The effect of doping YBCO, especially with Ca, has been studied extensively [14]. The substitution of the Y^{3+} ion by Ca^{2+} is expected to increase the carrier density

by introducing one additional hole per substituted ion, provided that the substitution does not create compensating defects such as oxygen vacancies. The critical temperature decreases with increasing doping and can be lowered in thin films to around 50 K by 40% Ca substitution [14]. Fig. 1 shows the temperature dependence of the resistivity of an epitaxial c-axis-oriented $Y_{0.7}Ca_{0.3}Ba_2Cu_3O_{7-\delta}$ film. This film was deposited by laser ablation on a $LaAlO_3$ substrate at 780 °C in 400 mTorr of O_2 and was then cooled in 600 Torr of O_2. X-ray diffraction shows no impurity-phase peaks, and the measured lattice constant in the growth direction is about 11.8 Å. The resistivity of the Ca-doped YBCO is lower than YBCO by roughly the amount expected from the increased carrier density; $T_c(R = 0)$ is about 50 K. However, the zero-resistance T_c of our unpatterned and identically deposited $Y_{0.7}Ca_{0.3}Ba_2Cu_3O_{7-\delta}$ films varies randomly between 40 K and 60 K. In addition, Appelboom et $al.$ [14] have reported a T_c of 60 K for fully-oxygenated $Y_{0.7}Ca_{0.3}Ba_2Cu_3O_{7-\delta}$ films fabricated by co-evaporation, and Kucera et $al.$ [15] found a T_c of 83 K for annealed sputtered $Y_{0.7}Ca_{0.3}Ba_2Cu_3O_{7-\delta}$ films. Since Ca-doped YBCO is known to be oxygen deficient, this wide variation probably reflects the high sensitivity of T_c to the oxygen concentration in this material [15, 16] . The T_c of Ca-doped YBCO films is also quite sensitive to the oxygen pressure used during the cooling of the sample. For example, cooling our laser-ablated films in an oxygen pressure of 5 Torr increases the T_c to ~80 K.

Fig. 2 shows the geometry of our SNS edge junctions. The YBCO/Ca-doped YBCO/YBCO junctions were fabricated by the same process used for our previously-described $CaRuO_3$ junctions [6]. Epitaxial layers were grown by laser ablation on a YSZ substrate with a CeO_2 buffer layer. Thicknesses of about 2000 Å for both the YBCO electrodes and the $SrTiO_3$ insulating layer were obtained. Patterning was accomplished by Ar ion-beam milling to obtain five 4-μm-wide junctions per chip. According to cross-sectional scanning electron microscope studies, the angle of the

slope of the first YBCO edge is about 20° to the plane of the substrate. In order to test the YBCO surface after the ion milling, we made an edge junction structure with no barrier layer. The critical current density was higher than 1×10^6 A/cm^2 at 77 K, suggesting that the ion-beam damaged YBCO surface was restored during the heating for the second YBCO deposition. The quality of the SrTiO$_3$ insulating layer was tested by making a few junctions with a 100 Å thick barrier of SrTiO$_3$. These junctions did not show any zero-voltage current, even though the resistance of the junctions varied between tens of ohms and hundreds of kilohms.

III. Results

Fig. 3 shows the current-voltage (*I-V*) characteristics of a 4-μm-wide junction with a 400 Å thick barrier of Ca-doped YBCO at several temperatures. At high temperatures, when the critical current is lower than 500 μA, the *I-V*s were found to be fit quite well by the simple resistively-shunted-junction (RSJ) model. Upon cooling, the *I-V*s start to quickly deviate from the RSJ model and show an excess current. This may be due to the self-field effect when the width of the junction becomes much larger than the Josephson penetration depth [17]. A critical current of 1 mA corresponds to $J_c = 1.2 \times 10^5$ A/cm^2, which makes the Josephson penetration depth $\lambda_J = \{ h/2e\mu_0(2\lambda+d)J_c\}^{1/2} = 1$ μm. This value is smaller than the junction width of 4 μm. However, it is not clear whether our SNS geometry is described by an overlap geometry or an in-line geometry as discussed by Barone and Paterno [18]. At lower temperatures, when the critical current is higher than ~5 mA, the *I-V* becomes a flux-creep-like curve, even above the bulk T_c of 50 K we have measured on our unpatterned Ca-doped YBCO films. We found that the crossover to flux-creep behavior depends on the magnitude of the critical current rather than the temperature.

This junction was also tested at 77 K in a magnetic field and under microwave radiation. When the magnetic field is applied in the direction perpendicular to the substrate, we observe the characteristic diffraction pattern of $I_c(H)$ with a central peak and an I_c modulation with a period of 0.15 Gauss as shown in Fig. 4. We do not understand quantitatively what diffraction pattern should be expected for the edge junction geometry because of the overlap of the second YBCO film, the anisotropy of the materials, and the flux focusing effect [19]. The part of the second YBCO that overlaps the junction may shield the initial applied magnetic field, resulting in an apparent shift of the magnetic field value where the critical current is maximum. Microwave irradiation modulates the critical current, and all the junctions show well-defined Shapiro steps as shown in Fig. 5.

The temperature dependence of the critical current for junctions with 200 Å, 400 Å, and 600 Å thick barriers is displayed in Fig. 6(a). The two sets of data for each barrier thickness represent junctions with the maximum and the minimum critical current of the five on a single chip. The temperature dependence of the critical currents shown in this figure is completely different from the dependence observed in most high-T_c Josephson junctions, for which a quasi-linear dependence over a wide temperature range is usually reported. The critical currents we observe are also higher than the critical currents reported in other YBCO-based junctions. For instance, the critical current for a barrier of 400 Å is as high as 9×10^4 A/cm^2 at 77 K, which can be important for applications requiring a high J_c.

Figure 6(b) displays the temperature dependence of the junction resistance R_n for the previous junctions. The resistances were determined by the slope in the linear part of the I-V curve at a bias current of roughly five times I_c. The samples with barriers of 200 Å and 400 Å show a linear increase of R_n with the temperature, but the data for the 600 Å sample show a slight structure around 80 K. This structure is highly reproducible over several junctions on different chips with the

same barrier thickness. We also note that the resistance does not scale well with the thickness of the barrier at high temperatures where the thinner barrier junctions have higher resistances than the bulk resistivity would predict. The dashed lines are the expected values of junction resistances for 200 Å, 400 Å and 600 Å thick barriers as calculated from the bulk resistivity in Fig. 1 and from the geometry. At temperatures near 75 K, the junction resistance (extrapolated for 200 Å) appears to scale well with the thickness. Most interestingly, it is obvious that the junction resistance decreases faster than the bulk resistivity would predict. For all thicknesses, the resistance is too high at high temperatures, correct near 75 K, and too low at low temperatures compared to the calculated values. As far as we know, this behavior has never been reported for high-T_c Josephson junctions which have high (10^{-8} $\Omega \cdot cm^2$) interface resistances. However, a similar behavior has been observed in the Co-doped YBCO based junctions [10, 11, 13], particularly for those with low doping levels. The origin of this temperature dependence of R_n is still not well established, even though Koren *et al.* explained this behavior by the flow of Josephson vortices in the junctions [11]. In the following sections we will offer alternative interpretations for the observed temperature dependence of R_n.

IV. Analysis with the proximity effect

We will show in the following that the behavior of $I_c(T)$ can be explained if there is a proximity effect in the Ca-doped layer. De Gennes' theory for a conventional proximity effect predicts in the dirty limit and close to T_c [20] that

$$I_c = I_0(1-t)^2 \frac{\kappa d}{\sinh(\kappa d)} = \frac{18.5 \text{mV}}{R_n}(1-t)^2 \frac{\kappa d}{\sinh(\kappa d)}, \tag{1}$$

where $t = T/T_c$, $I_0 = \pi\Delta_0^2 / 4eR_nk_BT_c$, d is the thickness of the barrier, and κ^{-1} is the decay length. In the case of a BCS gap, $2\Delta_0 = 3.52 k_BT_c$, and for $T_c = 89$ K, $I_0 = 18.5$ mV/R_n. In the absence of definite knowledge of the superconducting gap value, we used a prefactor that will generate a voltage scale close to a presumed superconducting gap value of YBCO, 20 mV. Even though the relation of Eq. (1) was originally derived in the dirty limit near T_c, as a first attempt to fit the general temperature dependence of the critical current over the entire temperature range, we will use Eq. (1) as a generalized form. Since the electronic mismatch between YBCO and Ca-doped YBCO is not significant, we used a $(1-t)^2$ dependence, which assumes continuous boundary conditions of the wave function and its derivative [1]. However, we also tried to fit our data with the $(1-t)$ dependence characteristic of tunnel junctions. It is obvious that the fitting is not as good as the $(1-t)^2$ case, especially for temperatures close to T_c where the $(1-t)$ or $(1-t)^2$ factor is dominant, since in this range the fit is relatively insensitive to the length dependence [21]. This is in contrast with the recent analysis of our data [e.g. that in Fig. 6(a)] by Kleinsasser and Delin [22], who used a $(1-t)$ dependence by assuming rigid boundary conditions as in tunnel junctions.

When the barrier material has a superconducting transition at T_n, the decay length is expressed in the dirty limit by

$$\kappa^{-1} = \left(D\frac{\hbar}{2\pi k_B T}\right)^{1/2}\left(1+\frac{2}{\ln(T/T_n)}\right)^{1/2}, \qquad (2)$$

where the diffusion constant $D = v_f l/3$, and l is the electronic mean free path. For the clean limit the decay length can be expressed [1] within the Ginzburg-Landau theory by

$$\kappa^{-1} = \sqrt{2} \times 0.74\, \xi_0\, (T/T_n - 1)^{-1/2}, \qquad (3)$$

where $\xi_0 = \hbar v_F / \pi\Delta$ is the BCS coherence length. We have used a temperature-independent resistance for the fitting, since the origin of the temperature-dependent resistance is not clear at this time. We will discuss this issue in the next section of this paper. As in the Co-doped YBCO system, the fits using the dirty limit [Eq. (2)] and the clean limit [Eq. (3)] are the same. This is not surprising since it is easy to show that Eq. (2) can be modified to $\kappa^{-1} \propto (T/T_n - 1)^{-1/2}$ when T is near T_n, where even the dirty limit formula is expected to follow the Ginzburg-Landau relation. In order to determine in which limit are the Josephson junctions with Co-doped YBCO barriers, we have looked at the variation of ξ_0 and D with the Co doping [13]; the data are consistent with the barriers with low Co doping (4% and 7%) being in the clean limit, and the barrier can be described by the dirty limit formalism when the Co doping is 14%. However, in the present study this procedure is not applicable because we have studied only one Ca doping level owing to the difficulty of controlling compensating defects. We will show that we can still determine the limit of the barrier by comparing the Co-doped and the Ca-doped system.

In the clean limit [Eq.(3)] the I_c values have been fitted with L being the only parameter, where the dimensionless L is defined by $\kappa d = L(T/T_c)^{1/2}$. The fitting lines shown in Fig. 6(a) have been calculated with T_n= 60 K and with $L = 3.3$, 7.4, and 12.9 (for a barrier thickness of $d = 200$ Å, 400 Å, and 600 Å) which correspond to an average coherence length $\xi_0 = 52$ Å. For each barrier thickness, L is an average value of the fitting parameter used on the two sets of data. This gives a decay length as high as 100 Å at 77 K, which is also the normal coherence length we estimated from the exponential decrease of the critical current with the thickness. We can compare this value to $\xi_0 = 30$ Å obtained for the clean 4% Co-doped YBCO which has a critical temperature T_c= 50 K, similar to the Ca-doped YBCO. From these measurements and with $\xi_0 = \hbar v_f / \pi\Delta$, the ratio between the Fermi velocity v_f (Ca)

and v_f(Co) should be 1.7 which corresponds to a ratio of 3 (in the case of 2D system) or 5.2 (in a 3D system) in the carrier density n (if we assume that it is valid to use the free electron model to estimate n from v_f). Carrington et al. [23] have reported Hall measurements on Co-doped single crystals which show that the ratio between the carrier density of YBCO and that of the 4% Co-doped YBCO is about 3.5. For the Ca-doped system, the carrier density is sensitive to the oxygen concentration [15], but if we assume that the only reason our films have a T_c of 50–60 K is because they are overdoped, then we can roughly estimate the ratio between the carrier density in the Ca-doped YBCO and YBCO by using an empirical formula extracted from thermopower measurements of Obertelli et al. [24] and confirmed in Ca-doped YBCO thin films by Kucera et al. [15]. We found that this ratio is about 1.4, implying that the ratio n(Ca)/n(Co) is about 5, which is close to the value we have extracted from our fitting.

If the Ca-doped YBCO is in the dirty limit, where $\kappa d = L \left(\dfrac{T}{T_c} \right)^{1/2} \left(1 + \dfrac{2}{\ln(T/T_n)} \right)^{-1/2}$, the fitting of $I_c(T)$ with Eq. (2) and T_n= 60 K gives L = 5.7, 12.7, and 22 , corresponding to a diffusion constant $D = 7$ cm^2/sec. This value is a factor of 1.5 higher than the $D = 5$ cm^2/sec found for the dirty 14% Co-doped YBCO [13]. Since $D = v_f l/3$ and $l = m v_f /(e^2 n \rho_n)$, where ρ_n is the resistivity of the barrier, it can be easily shown that

$$\frac{D(Ca)}{D(Co)} = \left(\frac{n(Co)}{n(Ca)} \right)^{1/3} \frac{\rho_n(Co)}{\rho_n(Ca)} , \tag{4}$$

where the Ca index is for the Ca-doped YBCO and Co stands for the 14% Co-doped YBCO. The Co-doped YBCO resistivity ρ_n(Co) is about 800 $\mu\Omega\cdot$cm at 100 K compared to 60 $\mu\Omega\cdot$cm for the Ca-doped YBCO. From the data of Carrington et al. [23] we can extrapolate that the ratio n(Ca)/n(Co) is about 13 and then the ratio D(Ca)/D(Co)

should be 5.6, which is higher than the ratio 1.5 obtained from the fitting. The comparison with the Co-doped barrier then seems to indicate that our Ca-doped barrier is indeed in the clean limit, again in contrast with the recent analysis of our data by Kleinsasser and Delin [22] who found the Ca-doped YBCO barrier to be in the dirty limit. Our conclusion is also confirmed by the fact that the resistivity of the Ca-doped YBCO is lower than YBCO, which is known to be in the clean limit [25].

Turning now to the anomalous temperature dependence of R_n [Fig. 6(b)], we note that a somewhat similar observation of a fast decrease of junction resistance has been reported by Clarke et $al.$ [26] in low-T_c Pb-Ir-Pb junctions in which Ir is a superconductor with T_c of 57 mK. Following the argument made to explain the low-T_c system, we suggest that one explanation of the decrease of $R_n(T)$ we observe in our junctions may also be attributed to a proximity effect in the Ca-doped YBCO. According to the theory of the proximity effect, when a normal metal is in contact with a superconductor through a very clean interface, the pair potential Δ_n in the metal is either zero, if the electron-electron interaction $V_n = 0$, or decreases exponentially from the value Δ_{ni} at the interface if $V_n > 0$. We now consider a current flowing through the S-N interface and an electron coming from the N side. Andreev reflection, the conversion of normal current to superconducting current, occurs at the point where Δ_n is equal to the energy of this electron. If $V_n = 0$, the Andreev reflection takes place at the interface, and in this case the resistance of the junction is expected to be equal to the bulk resistance of the N layer. This was observed for Pb-Cu-Pb junctions [27]. On the other hand, when the barrier itself is a superconductor and $V_n > 0$, the Andreev reflection takes place inside the N layer and the junction resistance should be less than the bulk N layer resistance. For this situation Clarke et $al.$ developed a simple model for a conventional proximity effect and found that the resistance increases logarithmically with temperature, which was in very good agreement with the experimental results for Pb-Ir-Pb [26]. However,

March 20, 1995

our data show that the junction resistance varies almost linearly with the temperature. This difference could be due to stronger coupling in our case, where J_c is very high, in contrast to the case of the Pb-Ir-Pb junctions where the coupling is very small and J_c is zero. Although Clarke *et al.* were able to quench the induced gap in the barrier at a few μV, we did not observe such an effect up to a couple of hundred μV. This could be due to the difference in the interaction potential in Ir (T_c= 57 mK) and Ca-doped YBCO (T_c= 50 K). We also note that this model for R_n cannot explain the fact [Fig. 6(b)] that for all thicknesses of the barrier, R_n is higher than expected for temperatures in the range 75 to 88 K.

V. Analysis using a diffusion model

Another possible explanation of $R_n(T)$ is that there is diffusion of the Ca from the barrier layer into the electrodes. For example, Fig. 7(a) shows the ideal 30% Ca doping profile uniformly distributed across the barrier thickness d compared to a proposed diffused profile in which the Ca distribution is a Gaussian with a full width at half maximum of d. Because the amount of Ca is the same in both cases, the maximum doping for the Gaussian profile is 28.2%. This doping profile results in a T_c distribution throughout the barrier as shown in Fig. 7(b). Note that in this model we assume a uniform distribution along the width of the junction, i.e. the diffusion results in a varying Ca composition only transverse to the barrier. This T_c profile has the following consequences. At high temperatures T close to T_c, if the effective barrier thickness is defined as the thickness of material with $T_c<T$, then the barrier is thicker than the nominal deposited Ca doped layer. At lower temperatures, using the same definitions, the barrier is thinner than the deposited layer. Hence at high temperatures the junction resistance will be larger than expected, while at low temperatures the resistance will be smaller. This is what we

observe. The data of Fig. 6(b) suggest that near 75 K, the barrier thickness is comparable to the deposited layer thickness, since the resistances scale appropriately with deposited thickness at that temperature.

In this diffusion model, we still rely on the proximity effect for the temperature dependence of the critical current. Since the effective thickness of the barrier depends on temperature, and T_c is not uniform transverse to the barrier, it is difficult to calculate the exact temperature dependence of the critical currents. However, we do not expect the overall shape of $I_c(T)$ to be altered significantly from what Eq. (1) predicts. We are currently in the process of investigating the interface diffusion issue with transmission electron microscopy.

We can further extend this model to take into account the possibility of doping variations in the lateral direction of the barrier. We discuss this "percolation model" in the following section.

VI. Analysis using a percolation model

Although the $I_c(T)$ data of the Ca-doped barrier junctions may be described by conventional proximity effect theory, this observation is only one of many relating to our devices which we do not in fact completely understand. Examples include the temperature dependence of the resistivity of oxygen-deficient and doped YBCO, the role of anisotropy in the edge junction devices, a detailed understanding of the I-V characteristics and the magnetic field diffraction patterns, the nature of the interface, non-reproducibility of I_c and R_n, and even whether YBCO is BCS-like or not. Thus, a high-T_c proximity effect is hardly proved. As has often been the case in the high-T_c arena, we turn again to phenomenological models to guide our thinking, particularly for improved junction devices. We are mindful of the considerable evidence suggesting that oxygen-depleted YBCO is inhomogeneous

with respect to its superconducting properties. Studies have shown that the superconductivity throughout microscopic regions of carrier-depleted thin-film YBCO is of a filamentary nature [9, 28]. Indeed, this is the reason why an elimination of excess interface resistance in high-T_c junctions was originally desired as a way to obtain uniform device characteristics [8].

Therefore, a very important question regarding the SNS junctions is the role played by the inhomogeneities in the doped YBCO system. We have already pointed out that the properties of Ca-doped YBCO are particularly sensitive to both the Ca concentration and the oxygen concentration. If, as the evidence suggests, the Ca-doping or the oxygen concentration or the carrier density are not homogeneous inside the junction barrier, we can represent this barrier by a set of grains with different T_c, as shown in Fig. 8 (these grains may or may not correspond to the actual crystalline grains forming the thin film). As we can see from the particular model in Fig. 8, when three adjacent grains that traverse the barrier become superconducting, a new filamentary superconducting path is formed which is a weak link (or can be formed by weak links) and which gives rise to the critical current of the junctions. The nature of the weak coupling of these filaments is puzzling, though no more so than for well-researched but still ill-understood grain boundary junctions. The dependence of the supercurrent on temperature can be predicted within this percolation-like model.

We derive a very simple relation by first assuming that the distribution $D(T)$ of T_c inside the Ca-doped YBCO barrier is linear between a temperature T_{min} and T_{max} with the simple form

$$\mathcal{D}(T) = C(1 - \frac{T}{T_{max}}) \tag{5}$$

which is represented in Fig. 9(a). Assumption of a different distribution, e.g. Gaussian, does not significantly affect the results of the model. The value of D(T) shown in this figure represents the probability of finding a grain with a critical temperature of T. Then the probability $P(T)$ to have superconducting grains at this temperature is represented by the shaded area between T and T_{max}. It is easy to show that if

$$P(T) = \int_{T}^{T_{max}} \mathcal{D}(t)dt \quad \text{and} \quad 1 = \int_{T_{min}}^{T_{max}} \mathcal{D}(t)dt, \tag{6}$$

this probability is

$$P(T) = \frac{(T_{max} - T)^2}{(T_{max} - T_{min})^2}. \tag{7}$$

$P(T)$ is shown in Fig. 9(b) for a linear distribution of T_c between T_{min} and T_{max}. In order to have a superconducting path through the barrier, n aligned grains should be superconducting, where $n = d/d_{grain}$, d is the barrier thickness, and d_{grain} is the grain size. In this percolation model, the probability to have n grains aligned is $P^n(T)$, and the critical current of the junction is then

$$I_c(T) = J_c(T)AP^n(T), \tag{8}$$

where $J_c(T)$ is the critical current density and $A = 8 \times 10^{-9}$ cm^2 is the area of the junction in our edge geometry. We will assume that the critical current density is that of bulk YBCO, i.e. it decreases linearly with temperature, $J_c = J_0 (1-T/T_c)$, where $T_c = 90$ K. We fix $J_0 = 2 \times 10^7$ A/cm^2, which corresponds to a reasonable value of $J_c = 3 \times 10^6$ A/cm^2 at 77 K. The results of the fitting with the percolation model are shown

in Fig. 10. The data for all barrier thicknesses are fit nicely. The averages of T_{min} and T_{max} for each pair of curves are found to be 61.7 K and 88.4 K for the 200 Å barrier, 57.1 K and 88.9 K for the 400 Å barrier, and 54.7 K and 82.2 K for the 600 Å barrier. From these values we can estimate that T_c in the Ca-doped barrier is distributed from T_{min} = 58 K to T_{max} = 86 K, which is consistent with the variation in the value of T_c observed in the Ca-doped system [15]. We have used for this fitting n = 1, 2, and 3 for the 200 Å, 400 Å, and 600 Å barrier thickness, respectively, which means that the size of the grains in the model is roughly 200 Å. As enough grains become superconducting and the regions of filamentary superconductivity become large, the weak coupling will be lost and flux-creep I-V characteristics will be observed, as we have mentioned to be the case.

If we take into account the effect of a different T_c for each individual superconducting filament on the temperature dependence of the critical current, the I_c (T) relation will be described by

$$I_c(T) = A \int_{T_{max}}^{T} \left[\frac{dP^n(T_c)}{dT_c} J_0 \left(1 - \frac{T}{T_c} \right) \right] dT_c. \qquad (9)$$

One can easily see that Eq. (9) becomes Eq. (8) if one ignores the dependence of $J_0(1-T/T_c)$ on the T_c variation. The curves obtained by fitting with Eq. (9) are very similar to the curves presented in Fig. 10 and calculated with Eq. (8). The only difference is a slight change in the two fitting parameters; T_{min} and T_{max} increase to 72.7 K and 89 K for the 200 Å barrier, 66.8 K and 89.5 K for the 400 Å barrier, 62.2 K and 83.5 K for the 600 Å barrier.

One difference between these devices and grain boundaries or other types of high-T_c junctions is the greater thickness of the effective "barrier" giving rise to the Josephson behavior, i.e. the entire doped-YBCO interlayer is important, rather than

the disordered region near a YBCO/YBCO or YBCO/metal interface. The regions of filamentary superconductivity are relatively larger in the present case, however, and there is little or no strain to prevent complete superconductivity at lower temperatures, hence the sharp rise in I_c with $(T-T_n)$. We should mention that because of this larger length scale, this simple model alone may not explain the Josephson behavior. A proximity effect between the superconducting grains may still play a role.

We can also explain qualitatively the behavior of the junction resistance with temperature within the percolation model, in terms of non-connected but superconducting grains. When the temperature is decreased from 90 K, a fraction of the grains will become superconducting, and it is likely that the current will preferentially flow through these regions. The presence of these superconducting grains in the middle of the current path will therefore effectively result in lower resistance. As the fraction of these superconducting regions increases with decreasing temperature, the resistance will decrease faster than the bulk resistance of the barrier. This is consistent with the observation that the rapid increase of critical currents corresponds to the points where the resistances extrapolate to zero (see Fig. 6).

VII. Conclusions

In section III we reported the electrical properties of SNS Josephson junctions based on YBCO with $Y_{0.7}Ca_{0.3}Ba_2Cu_3O_{7-\delta}$ barriers. We found that the critical current of these junctions has a temperature dependence which is not the usual quasi-linear dependence observed in most high-T_c junctions. Furthermore, the junction resistances R_n decrease faster with decreasing temperature than the resistance calculated from the resistivity of Ca-doped YBCO thin films. In sections IV, V, and

VI we described three models which can explain the data presented in the previous section. We showed in section IV that the $I_c(T)$ curves can be fitted and $R_n(T)$ qualitatively understood within the de Gennes theory. However, the $R_n(T)$ can be better understood qualitatively if one assumes diffusion between the barrier and the electrodes as described in Section V. On the other hand, those temperature dependencies can also be explained by a very simple percolation model in which the junction barrier is formed by grains with different critical temperatures, as discussed in section VI.

At this point it is not clear which model describes the real behavior of our Josephson junctions. Certainly, the fast increase of the critical current alone does not seem to guarantee the proximity effect, especially in this complicated materials system. We also note that the proximity theory is not explicably consistent with some of our other observations, and the diffusion and percolation models are phenomenological only. The degree of homogeneity of the barrier may determine which mechanism explains the junction properties, and it will certainly determine the uniformity and transport properties of the devices. It is possible that multiple mechanisms are involved.

From the technological point of view, these Josephson junctions with Ca-doped barriers may be useful for applications that require high values of J_c. However, a serious limitation is the high sensitivity of T_c to oxygen concentration and/or Ca distribution, which could affect the reproducibility of the junctions. Other limitations include an excessive J_c, a rapid variation of J_c with T, and an insufficient R_nA for junctions made by regular optical lithography (i.e., junctions larger than 2 μm in width).

March 20, 1995

REFERENCES

1.   E. Polturak, G. Koren, D. Cohen, E. Aharoni, and G. Deutscher, Phys. Rev. Lett. **67**, 3038 (1991).

2.   P. Chaudhari, and S.-Y. Lin, Phys. Rev. Lett. **72**, 1084 (1994).

3.   A. G. Sun, D. A. Gajewski, M. B. Maple, and R. C. Dynes, Phys. Rev. Lett. **72**, 2267 (1994).

4.   D. A. Wollman, D. J. Van Harlingen, J. Giapintzakis, and D. M. Ginsberg, Phys. Rev. Lett. **74**, 797 (1995).

5.   R. H. Ono, J. A. Beall, M. W. Cromar, T. E. Harvey, M. E. Johansson, C. D. Reintsema, and D. A. Rudman, Appl. Phys. Lett. **59**, 1126 (1991).

6.   K. Char, M. S. Colclough, T. H. Geballe, and K. E. Myers, Appl. Phys. Lett. **62**, 196 (1993).

7.   L. Antognazza, K. Char, T. H. Geballe, L. L. H. King, and A. W. Sleight, Appl. Phys. Lett. **63**, 1005 (1993).

8.   K. Char, L. Antognazza, and T. H. Geballe, Appl. Phys. Lett. **63**, 2420 (1993).

9.   B. H. Moeckly, D. K. Lathrop, and R. A. Buhrman, Phys. Rev. B **47**, 400 (1993).

10.   K. Char, L. Antognazza, and T. H. Geballe, Appl. Phys. Lett. **65**, 904 (1994).

11.   G. Koren, and E. Polturak, Physica C **230**, 340 (1994).

12.   Q. X. Jia, D. Reagor, S. R. Foltyn, M. Hawley, C. Mombourquette, K. N. Springer, and X. D. Wu, Physica C **228**, 160 (1994).

13.   L. Antognazza, S. J. Berkowitz, T. H. Geballe, and K. Char, to appear in Phys. Rev. B , (1 April 1995).

14.   H. M. Appelboom, H. Sato, and M. Naito, Physica C **221**, 125 (1994).

15.   J. T. Kucera, and J. C. Bravman, to appear in Phys. Rev. B , (1995).

16.   G. Xiao, and N. S. Rebello, Physica C **211**, 433 (1993).

17.   J. Clarke, Phys.Rev. **B4**, 2963 (1971).

18.   A. Barone, and G. Paterno, *Physics and applications of the Josephson effect.* (John Wiley & Sons, New York, 1982).

19.   P. A. Rosenthal, M. R. Beasley, K.Char, M. S. Colclough, and G. Zaharchuk, Appl. Phys. Lett. **59**, 3482 (1991).

20.   P. G. de Gennes, Rev. Mod. Phys. **36**, 225 (1964).

21.   S. J. Berkowitz, L. Antognazza, K. Char, R. H. Ono, N. Missert, P. A. Rosenthal, L. R. Vale, P. M. Mankiewich, and W. J. Skocpol, Submitted to Phys.Rev.B , (1995).

22.   A. W. Kleinsasser, and K. A. Delin, Appl. Phys. Lett. **66**, 102 (1995).

23.   A. Carrington, A. P. Mackenzie, C. T. Lin, and J. R. Cooper, Phys. Rev. Lett. **69**, 2855 (1992).

24.   S. D. Obertelli, J. R. Cooper, and J. L. Tallon, Phys.Rev.B **46**, 14928 (1992).

25.   K. Kamaras, S. L. Herr, C. D. Porter, N. Tache, D. B. Tanner, S. Etemad, T. Venkatesan, E. Chase, A. Inam, X. D. Wu, M. S. Hedge, and B. Dutta, Phys. Rev. Lett. **64**, 84 (1990).

26.   J. Clarke, S. M. Freake, M. L. Rappaport, and T. L. Thorp, Solid State Comm. **11**, 689 (1972).

27.   J. Clarke, Proc. Roy. Soc. **A308**, 447 (1969).

28.   B. H. Moeckly, R. A. Buhrman, and P. E. Sulewski, Appl. Phys. Lett. **64**, 1427 (1994).

FIGURE CAPTIONS

Figure 1.   Temperature dependence of resistivity for a 1000 Å thick $Y_{0.7}Ca_{0.3}Ba_2Cu_3O_{7-\delta}$ thin film on a $LaAlO_3$ substrate measured on an unpatterned film of 1/4" x 1/4" size.

Figure 2.   Schematic cross-sectional drawing of the edge junction geometry. Both of the YBCO electrodes are 2000 Å thick.

Figure 3.   Current-voltage curves of a YBCO / 400 Å Ca-doped YBCO / YBCO edge junction at several temperatures. The width of the junction is 4 µm.

Figure 4.   Critical current of a YBCO/ 400 Å Ca-doped YBCO/YBCO edge junction as a function of an applied DC magnetic field at 77 K.

Figure 5.   I-V characteristic under 3.5 GHz microwave radiation and at 77 K for the same device shown in Fig. 4.

Figure 6.   (a) Critical current and (b) junction resistance as a function of temperature for junctions with Ca-doped YBCO barriers of thickness 200 Å, 400 Å, and 600 Å. In (a) the solid lines are the fits using the proximity effect theory described in the text. The fitting within the clean limit and the dirty limit are overlapping. In (b) the dashed lines represent the calculated values of the 200 Å, 400 Å, and 600 Å thick barrier resistance using the resistivity of the Ca-doped thin film.

Figure 7.   (a) Gaussian distribution of Ca doping throughout the barrier region of thickness d assumed in the diffusion model. The dashed lines indicate the

nominally ideal Ca profile.   (b) The consequent distribution of T_c in the barrier region due to the Ca doping profile. A T_c of 75 K obtains at the thickness d of the nominal barrier.

Figure 8.   Schematic drawing of the edge junction. In the percolation model the barrier is represented by a set of grains with different T_c. The shaded grains represent the formation of a filamentary superconducting path.

Figure 9.   (a) Linear distribution D(T) of critical temperature in the Ca-doped YBCO barrier used in the percolation model. The shaded area represents the probability to have grains with a critical temperature at or above T. (b) Probability $P(T)$ to find grains which are in the superconducting state at a given temperature T.

Figure 10.   Critical current as a function of the temperature for junctions with Ca-doped YBCO barriers of thickness 200 Å, 400 Å, and 600 Å. The solid lines represent the fit of I_c with the percolation model.

Fig. 1

Ca doped YBCO

SrTiO$_3$

YBCO

CeO$_2$ →

YBCO

YSZ substrate

Fig. 2

Fig. 3

Fig. 4

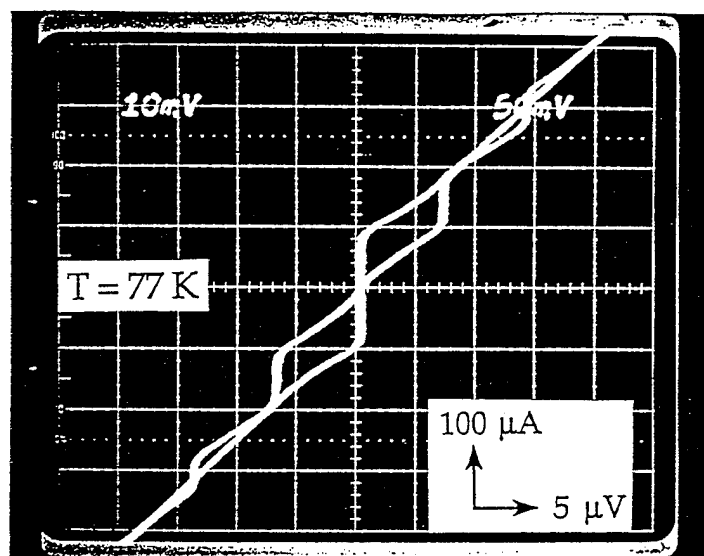Fig. 5

Fig. 6

local doping
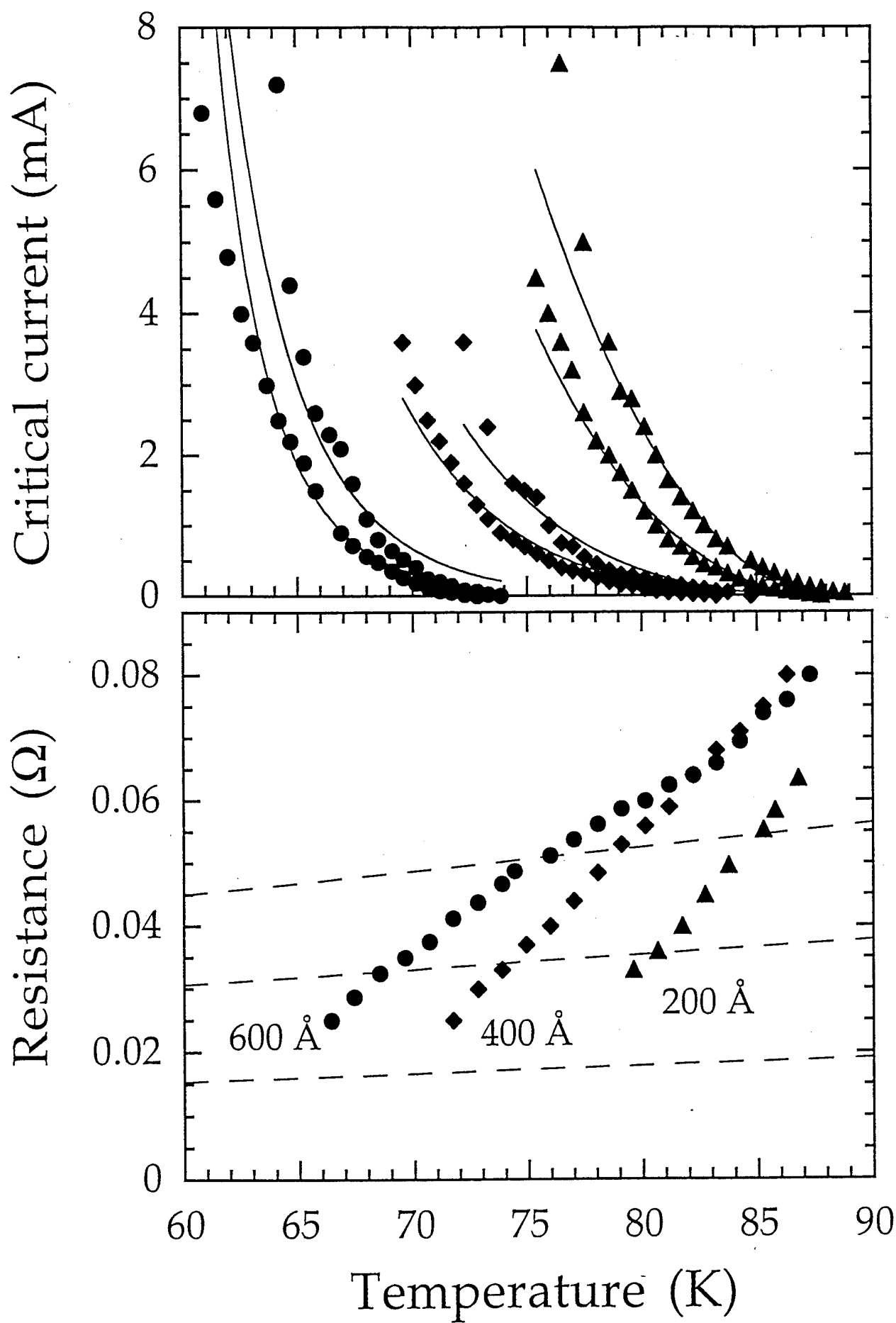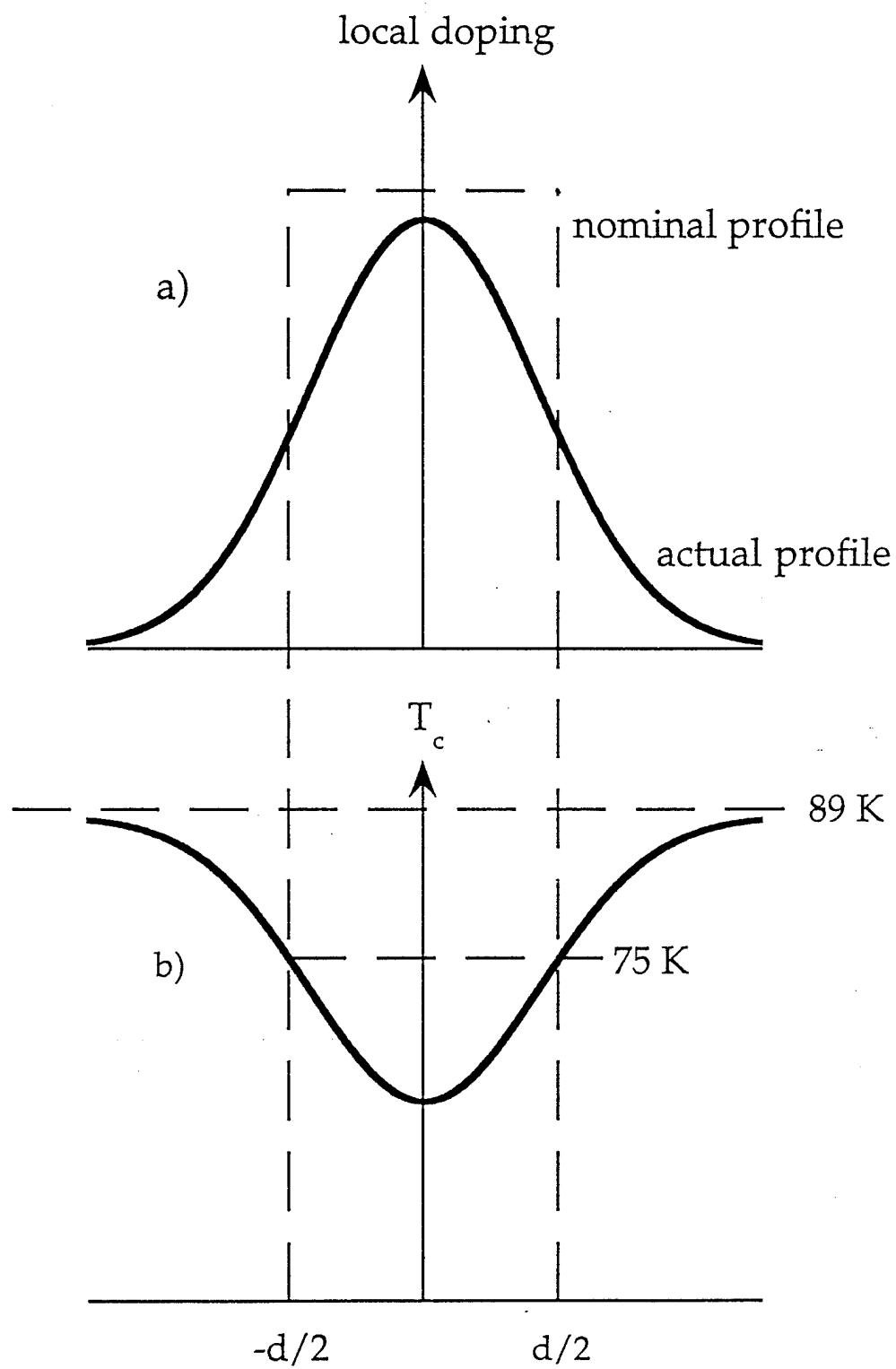
a)

nominal profile

actual profile

T_c

b)

89 K

75 K

-d/2   d/2

Fig. 7

Ca-doped YBCO

YBCO

YBCO

Fig. 8

(a)

$\mathcal{D}$(T)

T_{min} T T_{max}

(b)

P (T)

1

0.8

0.6

0.4

0.2

0

T_{min} T_{max}

Temperature (K)

Fig. 9

Fig. 10